Dissociative iodomethane adsorption on Ag-MOR and the formation of AgI clusters: An ab initio molecular dynamics study

T. Bučko, S. Chibani, J.-F. Paul, L. Cantrel, M. Badawi

Dissociative iodomethane adsorption on Ag-MOR and formation of AgI clusters: an ab-initio molecular dynamics study

Tomáš Bučko,*,†,‡ Siwar Chibani,¶,§ Jean-Francois Paul,§ Laurent Cantrel,‖ and Michael Badawi¶

Department of Physical and Theoretical Chemistry, Faculty of Natural Sciences, Comenius University, Mlynská Dolina, SK-84215 Bratislava, SLOVAKIA, Institute of Inorganic Chemistry, Slovak Academy of Sciences, Dúbravska cesta 9, SK-84236 Bratislava, SLOVAKIA, Université de Lorraine, Laboratoire de Chimie et Physique - Approche Multi-Echelle des Milieux Complexes EA4632, Institut Jean-Barriol FR2843 CNRS, Rue Victor Demange, 57500 Saint-Avold, FRANCE, Université de Lille, CNRS, ENSCL, Centrale Lille, Univ. Artois, UMR 8181 - UCCS - Unité de Catalyse et de Chimie du Solide, F-59000 Lille, FRANCE, and Institut de Radioprotection et de Sûreté Nucléaire, CE Cadarache, F-13115 Saint Paul lez Durance, FRANCE

E-mail: bucko19@uniba.sk

July 23, 2017

Abstract

*To whom correspondence should be addressed

†Comenius University, Slovakia

‡Institute of Inorganic Chemistry, Slovak Academy of Sciences, Dúbravska cesta 9, SK-84236 Bratislava, SLOVAKIA

¶University of Lorraine, France

§Université de Lille, CNRS, ENSCL, Centrale Lille, Univ. Artois, UMR 8181 - UCCS - Unité de Catalyse et de Chimie du Solide, F-59000 Lille, FRANCE

‖Institut de Radioprotection et de Sûreté Nucléaire, France

Radioactive iodine species belong to the most dangerous components of nuclear effluents and waste produced by nuclear facilities and this fact motivates a significant effort in development of technologies for their efficient trapping. In this work we use computer simulations at the periodic DFT level to investigate dissociative adsorption of iodomethane on silver exchanged mordenite, which is among the most effective sorbents of iodine species available as of today. The structure, energetics, and mobility of complexes Ag-(CH_3I) and Ag-(CH_3I)$_2$ formed upon adsorption of iodomethane on Ag^+ sites are investigated using the ab-initio MD approach. The free-energy profiles for the reaction CH_3I + Ag-MOR $\rightarrow$ AgI + CH_3-MOR are determined using the blue moon ensemble technique. The AgI species formed as a product of dissociative adsorption are shown to combine spontaneously into small clusters $(AgI)_n$ with the dimensions restricted by the size and geometry of confining void. The structure and energetics of the $(AgI)_n$ species are analysed in detail and compared with the available experimental and theoretical data. The internal energy of formation of clusters in mordenite is shown to contribute significantly to the shift of equilibrium from undissociated to dissociated form of adsorbed CH_3I.

1 Introduction

The radioactive iodine compounds are present in effluents and waste of nuclear facilities only in relatively small amounts. Nevertheless, a very long half-life of radionuclide ^{129}I (17 million years[1]) and its involvement in metabolic processes[2] are the reasons why these species represent some of the most dangerous components of waste produced by nuclear installations. Furthermore, significant amounts of another dangerous radionuclide ^{131}I can be released into environment during a severe nuclear accident.[3] The iodine species present in nuclear effluents and waste include I_2, HI, and diverse organoiodides.[4] As a model system for the latter type of species, iodomethane (CH_3I) has often been considered in literature.[5–12] This species is formed in reactions of I_2 with organic impurities dissolved in water or with painted surfaces

.[4] Due to its high volatility and relatively low reactivity, iodomethane is more difficult to trap than other iodine containing compounds.[13]

Technologies for airborne iodine trapping discussed in the literature[4,9] employ several different sorbent types such as aqueous solutions, ceramics, aerogels, and metal-organic frameworks. In this work we focus on silver exchanged zeolite mordenite (MOR), which is among the most effective sorbents[5,7,8,11,12,14,15] available as of today: for Ag-MOR with the silver content of 9 weight percent, the reported adsorption capacity at 100°C is ∼120 mg/g.[12] Another important property of MOR with respect to the target application is that it can be prepared with relatively high Si/Al ratio, which improves its stability in the acidic waste streams.[8] Due to their great technological importance, the Ag-exchanged zeolites have attracted a significant research interest[5,8,12,14,15] but despite that, an atomistic scenario of adsorption and eventual conversion of iodine species over the Ag^+ sites is not yet fully developed. It is known that this process is dissociative and leads to the formation of clusters $(AgI)_n$ trapped in zeolite pores but, to the best of our knowledge, the mechanism of this transformation has not yet been examined. Recent papers published by Chibani et al.,[11,15] in which the energetics of the Ag^+ sites in MOR and their interactions with I_2 and CH_3I have been investigated, belong to few theoretical studies related to the subject.

The ability of the Ag-zeolites to form solid AgI clusters that are stable over long period of time makes these materials suitable for radioactive iodine storage applications. The nature of the $(AgI)_n$ clusters is relatively frequently discussed in literature.[8,14,16–18] Kodaira et al.[16] observed in their optical and X-ray diffraction experiments the formation of $(AgI)_2$, $(AgI)_3$, and $(AgI)_4$ clusters in the sodalite cages of zeolite LTA. For the latter cluster type, a cubic structure has been proposed as plausible[16,18] but this claim has not been supported by a direct evidence. A certain regularity in the distribution of the AgI clusters in the sodalite cages of zeolite A has been reported in X-ray diffraction study of Heo et al.[18] In the experimental work of Nenoff et al.,[8,14] radial distribution function (RDF) for the Ag-Ag, Ag-I and I-I pairs in $(AgI)_n$ created in Ag-MOR upon CH_3I adsorption was obtained on the

basis of X-ray diffraction experiment. By comparison with the RDF determined for three different stable crystalline phases of AgI, the $(AgI)_n$ clusters were identified as the phase α although the size of clusters determined from the shape of RDF was only $\sim$7 Å[14] and hence the clusters must have consisted of few AgI units only. Indeed, the size and geometry of confining voids represent limiting factors for the dimensions of clusters grown in the interior of zeolites. A typical number of AgI units in the $(AgI)_n$ clusters formed in MOR and several other zeolites reported in previous experimental work[10] is around four. No crystallographic ordering of clusters within the lattice of MOR has been observed.[14]

In this work we employ a state-of-art simulation methodology, based on a combination density functional theory with molecular dynamics, to investigate the atomistic details of processes related to the dissociative adsorption of iodomethane over Ag-MOR. In particular, we elucidate the mechanism of conversion of iodomethane into monomeric AgI unit and examine the structure and energetics of the $(AgI)_n$ clusters that are formed when several AgI units are combined together. This paper is organized as follows: in Sec. 2, technical aspects of our simulations are described, the reaction mechanism for the CH_3I transformation and its zero-temperature energetics are explored using static approach in Sec. 3.1, nature of the interaction iodomethane with adsorption site at the target experimental temperature is discussed in Sec. 3.2, finite temperature reaction energetics is investigated in Sec. 3.3, the structure and energetics of the $(AgI)_n$ clusters formed upon dissociative adsorption of CH_3I in Ag-MOR are analysed in Sec. 3.4, and the principal results of this study are summarized in Sec. 4.

2 Methodology and structural model

2.1 Electronic structure calculations

Periodic density-functional calculations have been performed using the VASP code.[19–22] The Kohn-Sham equations have been solved variationally in a plane-wave basis set using the

projector-augmented-wave (PAW) method of Blöchl,[23] as adapted by Kresse and Joubert.[24] The PBE exchange-correlation functional in the generalized gradient approximation proposed by Perdew et al.[25] was used. The $D2$ correction of Grimme[26] has been applied to account for long-range dispersion interactions that are not treated correctly by local and semilocal density-functional theory. This approach was shown to improve predictions on structure, energetics, and elastic properties of wide range of materials where dispersion forces play an important role.[27] As shown by Göltl et al.,[28] the PBE-D2 approach predicts reasonable adsorption energies (compared to experiment and advanced quantum-chemical calculations) for some of the zeolite-related applications. Owing to the large supercell used in calculations (see Sec. 2.4), Brillouin-zone sampling was restricted to the Γ-point. A plane-wave cutoff energy of 400 eV was used in all calculations.

2.2 Structural relaxations

First order saddle points of the potential-energy surface (i.e. transition states) have been identified using the dimer method,[29] as recently improved by Heyden et al.[30] Atomic positions were considered to be relaxed when all forces acting on the atoms were smaller than 0.005 eV/Å. The intrinsic reaction coordinates (IRC)[31,32] for the forward and backward reaction steps were identified using the damped velocity Verlet algorithm.[33] The structures corresponding to potential energy minima along the IRC were further relaxed using a conjugate-gradient algorithm[34] such as to satisfy the same optimisation criterion as for transition states. This procedure ensures that each reactant state is directly linked with corresponding transition state via a transformation path along which the energy changes monotonically.

Using the structural relaxations, the interaction energies between substrate (Ag-MOR) and n molecules of adsorbate have been computed using the following formula:

$$\Delta E_{int} = \frac{E_{zeo+n\times mol} - E_{zeo} - n \times E_{mol}}{n}, \tag{1}$$

where $E_{zeo+n\times mol}$ is the energy of relaxed interacting system (consisting of substrate and n adsorbate molecules), and E_{zeo} and E_{mol} are energies of relaxed clean substrate, and of a single non-interacting adsorbate molecule, respectively. We note that the interaction energy determined in this way can be considered as a classical zero-temperature limit of internal energy of adsorption.

The energy of formation of a cluster $(AgI)_n$ consisting of n AgI units has been determined using the following equation:

$$\Delta_f E = E_{(AgI)_n}/n - E_{AgI}. \tag{2}$$

with $E_{(AgI)_n}$ being the energy of the relaxed cluster and E_{AgI} is that computed for a single unit comprising the cluster.

2.3 Molecular dynamics simulations

Born-Oppenheimer ab-initio molecular dynamics (AI-MD) simulations have been performed in the NVT ensemble. The simulation temperature was controlled using a Nosé-Hoover thermostat[35,36] and its value was set to T=373 K. We note that this choice of temperature has been inspired by typical experimental and target operational conditions[9,10] and a similar temperature is expected to be reached in containment building during a severe nuclear accident.[37] The atomic mass of tritium has been used for all H atoms and a time-step of 1 fs has been used for the integration of the equations of motion.

The finite-temperature internal energy of adsorption has been computed as follows:

$$\Delta U_{ads} = \frac{\langle E_{zeo+n\times mol}\rangle_T - \langle E_{zeo}\rangle_T - n \times \langle E_{mol}\rangle_T}{n}, \tag{3}$$

where $\langle E_{zeo+n\times mol}\rangle$, $\langle E_{zeo}\rangle$, and $\langle E_{mol}\rangle$ are ensemble averages of total energies computed for the zeolite with the adsorbate, the clean zeolite, and the adsorbate in the gas phase, respectively. Similarly, the internal energy of formation of a gas-phase cluster consisting of

n units has been determined using the following equation:

$$\Delta_f U_{gas} = \frac{\langle E_{(AgI)_n} \rangle - n\langle E_{AgI} \rangle}{n}, \tag{4}$$

with $E_{(AgI)_n}$ being the total energy of the cluster in the gas-phase and E_{AgI} is that computed for a single gas-phase AgI unit. When the cluster was confined in the zeolite, the internal energy of formation was computed using:

$$\Delta_f U_{zeo} = \frac{\langle E_{\mathrm{zeo+(AgI)}_n} \rangle + (n-1)\langle E_{\mathrm{zeo}} \rangle - n\langle E_{\mathrm{zeo+AgI}} \rangle}{n}, \tag{5}$$

where $E_{\mathrm{zeo+(AgI)}_n}$ is the total energy of zeolite with cluster $(\mathrm{AgI})_n$, and $E_{\mathrm{zeo+AgI}}$ is the total energy of zeolite interacting with a single AgI unit.

The free-energy calculations are based on the blue moon ensemble method[38] implemented in VASP,[39] details of our approach are described in Appendix A.

2.4 Structural model

The crystal structure of mordenite (MOR) and the nomenclature used for the crystallographically inequivalent tetrahedral (T) and oxygen (O) positions (labelled as in Ref.[40]) are shown in Fig. 1. The possible positions of extra-framework cations catalogued by Mortier[41] are also displayed. A periodic structural model of mordenite based on the lattice geometry determined by Demuth et al.[42] using density-functional calculations has been used as a basis for construction of a supercell employed in this work. The computed[42] lattice constants for the conventional orthorhombic unit cell of purely siliceous MOR are in good agreement with the experimental values of Schlenker et al.[43] for protonated MOR: $a = 18.26$ (18.22) Å, $b = 20.71$ (20.47) Å, $c = 7.61$ (7.53) Å (experimental values in parentheses). In order to minimize any undesired interaction between the adsorbed molecule and its replicas in the periodically repeated cells, we have used an alternative representation with a primitive monoclinic cell doubled in the c-direction. The supercell used in our calculations is defined by the following

lattice parameters: $a = b$ =13.804 Å, c=15.212 Å, and $\beta = 82.8°$.

In the previous work of Chibani et al.,[15] a systematic analysis of energetics of all possible locations of Ag cations in MOR with the Si/Al ratio fixed at the value 47 has been performed. The Mortier position E located in the main channel has been found to be the energetically most favourable Ag^+ position for the iodomethane adsorption and this result inspired our choice of the structural model used in this work (see Fig. 2). Due to increased repulsive interactions of CH_3I with zeolite framework, the adsorption complexes formed in the side pocket and side channel were found to be significantly higher in energy compared to the adsorption complexes located in the main channel (the difference in energy being as large as 15-90 kJ/mol, see Ref.[15]). We therefore do not consider the Ag^+ sites in the side pocket and side channel in this study.

3 Results and discussion

3.1 Dissociation mechanism

As known from experiment,[5,8,10] the dissociation of CH_3I over Ag-MOR leads to the formation of AgI and a methoxy group, the latter being precursor for a number of subsequent reactions yielding products such as CH_4, C_2H_4, C_3H_6, C_3H_8, C_2H_6O, or CH_3OH.[10] Indeed, the chemistry of alkoxy species is well understood and the formation of the aforementioned products can be easily explained (see e.g. Ref.[44]). Hence we focus only on the much less well explored reaction step in which the C-I bond is broken. Two possible variants of the dissociation mechanism have been considered in the previous experimental work of Chebbi et al.[10] The first mechanism (I) involves Brønsted acid (BA) sites assumed to be present at non-negligible amounts in Ag-MOR.[10] The mechanism I proceeds via formation of reaction intermediate HI as follows:

$$CH_3I + \text{H-Zeo} \quad \rightarrow \quad HI + CH_3\text{-Zeo}$$

$$\mathrm{HI} + \text{Ag-Zeo} \quad \rightarrow \quad \mathrm{AgI} + \text{H-Zeo}$$

In the alternative mechanism (II), iodometane reacts directly with the Ag^+ site as follows:

$$\mathrm{CH_3I} + \text{Ag-Zeo} \quad \rightarrow \quad \mathrm{AgI} + \mathrm{CH_3}\text{-Zeo}$$

We note that a scenario analogous to the mechanism II was assumed in previous experimental[45] and theoretical[46] studies on conversion of CH_3I over alkaline-metal exchanged zeolites.

Geometry relaxations have been performed to examine the zero-temperature energetics for both alternatives, the resulting reaction energy profiles are shown in Fig. 3, while the structures of the corresponding stationary states on the potential energy surface (PES) are displayed in Figs. 4 and 5. As a reference state for our analysis of energetics of mechanism I, clean zeolite with a BA site and an isolated gas-phase CH_3I molecule are chosen. The BA site with Al in the position T1 and proton on neighbouring oxygen O7 (see Fig. 1) has been considered. Upon insertion of the reactant molecule into the main channel of mordenite, adsorption complex shown in Fig. 4(R1) is formed and the potential energy of system decreases to -74 kJ/mol. Similar values of interaction energies between CH_3I and various BA sites in the main channel of MOR have been reported also in our previous work[15] although a different approach for the long-range dispersion energy calculation within DFT has been used. In the transition state, methyl group forms a nearly flat configuration located between iodine and zeolite oxygen atom, see Fig. 4(TS1). The computed intrinsic reaction barrier (defined with respect to the adsorbtion complex) is 182 kJ/mol. In the product configuration, the HI molecule and a methoxy group linked to the Al-O-Si bridge are formed (see Fig. 4(P1)). This reaction is strongly endothermic ($\Delta_r E$=78 kJ/mol) and the energy of the product is 4 kJ/mol above the energy of the non-interacting reference state.

The isolated gas-phase iodomethane and a clean substrate (Ag-MOR) were used as a reference state also in our analysis of the mechanism II. When adsorption complex is formed, the number of bonds between the Ag^+ site and framework oxygen atoms is reduced from

four to two (cf. Fig. 2 and Fig. 5(R2)). The computed interaction energy is −145 kJ/mol and this value compares reasonably well with our previously published result of −152 kJ/mol obtained using the dispersion correction scheme TS/HI.[47,48] In transition state (Fig. 5(TS2)), the cation Ag^+ is completely detached from the zeolite framework and a nearly planar CH_3 group is located between iodine and the framework O atom next to Al. The computed intrinsic activation energy for this mechanism (136 kJ/mol) is much lower than that for the mechanism I, and the transtion state is 8 kJ/mol lower in energy than the reference state (see Fig. 3). In the product configuration (Fig. 5(P2)), a charge-neutral AgI unit that is not bound to the zeolite is formed and the methoxy group is attached to the Al-O-Si bridge. Similar to the mechanism I, this reaction is strongly endothermic ($\Delta_r E$=94 kJ/mol)) but the potential energy of the product configuration (−51 kJ/mol) is well below that of the reference state. A variant of the mechanism II, in which the methoxy group is formed at the Si-O-Si instead of the Al-O-Si bridge is described in Sec. SI of the Supporting Information.[49] This mechanism is energetically less favourable than the variant discussed here, which merely reflects the fact that the negative framework charge introduced by the Al→Si substitution is localized on the O atoms neighbouring aluminium and hence these atoms represent more favourable locations for the binding of the positively charged methyl group than other framework O sites.

Altogether, our results indicate that the mechanism II proceeds via much lower activation barrier than the mechanism I and it should therefore occur at a significantly higher rate. We therefore use only the mechanism II as a basis for our further analysis.

As an important modification of the mechanism II, reaction involving adsorption complex with two iodomethane molecules attached to a single Ag^+ site will be now considered. This is a highly relevant case because the experimentally reported average number of molecules per a single Ag^+ site in MOR is typically higher than one.[5,50] At the same time, we note that our attempts to create a stable adsorption complex with three molecules did not succeed and all such configurations collapsed during the structural relaxations. Our zero-temperature

simulations therefore suggest that the adsorption capacity of a single Ag^+ site is limited to two molecules and our finite-temperature calculations presented in Sec. 3.2 confirm this result. In Fig. 6, the energy diagram for the reaction involving two reactant molecules adsorbed at a single Ag^+ site is compared with that for the mechanism II with one molecule, and the structure of the corresponding stationary points are shown in Fig. 7. As a reference state, clean Ag-MOR and two non-interacting gas phase molecules of reactant are considered. Starting from the configuration R2 (one CH_3I is attached to Ag^+ and the other CH_3I is in the gas-phase), the total energy decreases by 74 kJ/mol when the second CH_3I is transferred from the gas phase to the Ag^+ site to form the configuration R4 (see Fig. 7). Hence the zero-temperature estimate for the adsorption energy (eq. 1) is -109 kJ/mol (per a molecule) which is significantly less than the value obtained for the adsorption of a single molecule (-145 kJ/mol). At the same time, the number of bonding contacts between Ag^+ and the framework O atoms is reduced from two to one (cf. Fig. 5 (R2) and Fig. 7 (R4)). Hence the decrease of adsorption energy is at least in part caused by the weakening of the interaction between Ag^+ and zeolite. The orientation and distances between iodine, the CH_3 group, and the framework O atom in the transition state are very similar to those found in the structure TS2 (cf. Fig. 5 (TS2) and Fig. 7 (TS4)). The computed activation energy is 98 kJ/mol, i.e. lower by $\sim$38 kJ/mol compared to the value computed for the reaction involving only one adsorbate molecule. As a product of dissociation, the methoxy group next to the framework Al and a free neutral IAg-I-CH_3 fragment are formed (see Fig. 7 (P4)). The total energy of this final configuration is 62 kJ/mol higher than that of the adsorption complex R4 and hence the reaction step R4$\rightarrow$P4 is much less endothermic than the corresponding step for the reaction involving only one adsorbate molecule (R2$\rightarrow$P2).

3.2 Interaction of iodomethane with the Ag^+ site

The nature of interaction of reactant with active site is an important factor affecting the mechanism and kinetics of chemical reactions. It is therefore useful to start our discussion

of finite temperature energetics of dissociation by exploring the behaviour of the active site and of adsorption complexes that it forms with the reactant molecule. Our analysis is based on a series of NVT molecular dynamics simulations (see Sec. 2.3 for details) performed for clean substrate, gas phase molecule, and adsorption complexes with one and two reactant molecules. The length of all MD runs discussed in this section is 100 ps, whereby the initial period of 5 ps is considered as equilibration and the corresponding data are not included in calculations of ensemble averages. As already mentioned in Sec. 2.3, the choice of simulation temperature of T=373 K has been motivated by experiment.[9,10,37]

Radial distribution functions (RDF) computed for the Ag-O pairs in the clean Ag-MOR, and in adsorption complexes with one or two reactant molecules are shown in Fig. 8. The RDF for the clean substrate exhibits its first maximum (reflecting the average nearest neighbour separation) at the distance of ∼2.4 Å while the first minimum (related to the size of the first coordination sphere of oxygen atoms around Ag) occurs at ∼3.1 Å. As obvious from the nearly vanishing value of RDF at the first minimum, the location of Ag^+ on the framework is stable, i.e. without frequent reconnections of the Ag-O bonds. The average coordination number computed from the RDF (see Sec. SII in the Supporting Information[49]) is 4.0 and this numerical result is confirmed by visual inspection of trajectory generated by MD: the motion of cation Ag^+ is strongly limited due to the presence of four bonds formed with the O atoms in the six-membered ring containing the Al atom (see Fig. 2).

The binding of Ag^+ to the framework O atoms is significantly weakened upon adsorption of iodomethane, which is evident from the visual inspection of the MD trajectory as well as from the change of the RDF computed for the Ag-O pairs (see Fig. 8). The first coordination sphere of O around Ag is still well defined but the average coordination number decreases from 4.0 (clean substrate) to only 1.0. At the same time, the position of the first peak is shifted from 2.4 Å to 2.2 Å and the first minimum shifts from 3.1 Å to 2.5 Å. These results indicate that the average number of the Ag-O bonds decreases due to the interaction with adsorbate but the remaining Ag-O bond becomes stronger. The adsorption complex

Ag-ICH_3 is thus relatively flexible but still firmly attached to at least one framework oxygen. Although our MD simulation was started from the relaxed configuration R2, the coordination of Ag^+ to the framework O atoms and the orientation of the Ag-ICH_3 complex in typical configurations observed in our MD simulation changed significantly compared to the result of relaxation: as shown in Fig. 9, the number of Ag-O bonds decreased from two to one and the methyl group was rotated by approximately 180° around the Ag-I axis. Interestingly, the relaxation of adsorption complex observed in MD led to a structure (R2') that is ∼11 kJ/mol higher in energy compared to the configuration R2 and this difference is at least in part due to the different number of Ag-O bonds in R2 and R2'. Hence the zero-T and the finite-T ground-states for this adsorption complex differ and the finite-T stabilization of configuration with higher potential energy must be accomplished via increased entropy. Clearly, the configuration R2' with fewer Ag-O bonds is more flexible and it is therefore favoured by entropy over the more ordered structure R2. The internal energy of adsorption computed using eq. 3 is −117 kJ/mol. As expected, this number is lower in absolute value than the zero-T estimate (−145 kJ/mol); this is partly due to the rearrangement of the adsorption complex discussed above and partly due to the fact that with increasing temperature, a flexible adsorption complex is less and less likely to be found in its energetically optimal orientation (as identified in static approach) with respect to the substrate. A similar effect has been reported e.g. for propane adsorbed in chabazite and mordenite.[51,52]

When a second CH_3I molecule is added, the interaction between Ag^+ and the framework O atoms is further weakened. Consequently, the adsorption complex Ag-$(CH_3I)_2$ is frequently detached from the framework for short periods of time during which it moves towards the centre of the channel. Furthermore, the CH_3I fragments in the adsorption complex Ag-$(CH_3I)_2$ rotate rather easily giving rise to a large variety of different configurations. This flexibility is illustrated by Fig. S3 in the Supporting Information[49] showing selected snapshots taken from the MD trajectory. The shape of RDF computed for the Ag-O pairs in this complex (see Fig. 8) reflects this newly acquired flexibility: position of the first peak is

shifted to ∼2.4 Å and the RDF at the first minimum (∼3.1 Å) takes a non-vanishing value of ∼0.6 indicating that the first coordination sphere of O atoms around Ag is not well defined. The increased flexibility of the adsorption complex also causes that any additional molecule is effectively prevented from approaching sufficiently close to the Ag^+ site to form a stable bond. We, indeed, did not succeed to create an adsorption complex with three adsorbate molecules that would be stable in MD simulations. In line with our zero-temperature result we conclude that the maximum adsorption capacity of a single Ag^+ site is two molecules and this result is also consistent with experiment.[5,50] Internal energy of adsorption computed using eq. 3 is −99 kJ/mol (per a molecule), which is to be compared with the our zero-temperature result of −109 kJ/mol. As expected on the basis of our static calculations, the contribution of the second adsorbate molecule to the total interaction energy (−81 kJ/mol) is significantly lower than that for the first molecule (−117 kJ/mol).

3.3 Finite temperature dissociation energetics

In this section we explore how the entropy and thermal effects affect the energetics of the dominant mechanism of the CH_3I dissociation identified in Sec. 3.1. The free-energy barrier ($\Delta A^{\ddagger}$) and the free-energy of reaction ($\Delta_r A$) for T=373 K have been computed using the blue moon ensemble MD as described in Appendix A, additional data used in calculations are compiled in Sec. SIV of the Supporting Information.[49] The partitioning of $\Delta A^{\ddagger}$ and $\Delta_r A$ into internal energy and entropy contributions has been done as explained in Appendix B. As an approximation of the reaction coordinate (ξ) the following geometric parameter has been used in our calculations:

$$\xi = r_{C-I} - r_{C-O_{Al}}, \tag{6}$$

where $r_{C-O_{Al}}$ is the interatomic separation between carbon atom in CH_3I and selected framework oxygen atom neighbouring Al, and r_{C-I} is the distance between carbon and iodine atoms in CH_3I. Note that the atom O_{Al} has been chosen so that the methyl group is formed

at the same position as in our zero-temperature calculations. In thermodynamic integration, 18 (reaction with a single CH_3I molecule) or 13 (two molecules) regularly distributed integration points separated by an increment of $\Delta\xi$=0.4 Å were used. Each point was sampled in a separate constrained MD run of length of 35 ps whereby the initial period of 5 ps was considered as equilibration. The values of ξ for the free-energy transition states were identified as the points with vanishing gradients in the computed $\left(\frac{\partial A}{\partial \xi}\right)_{\xi^*}$ vs. ξ dependence. For each transition state, a constrained MD run of length of 50 ps was performed in order to determine the terms needed for the calculations of free-energy and internal-energy of activation (see Appendix A and B).

The free-energy profile $A(\xi)$ for the reaction with one reactant per adsorption site is shown in Fig. 10(a). As an initial point for the thermodynamic integration, the point ξ=−4.45 was selected. This point is close to the maximum of the relatively narrow probability density $P(\xi)$ (see Fig. S6 in the Supporting Information[49]) determined for reactant using the MD run discussed in Sec. 3.2. We note that the configurations corresponding to this point are similar in structure to the configuration R2' shown in Fig. 9. The value of ξ in the free-energy transition state is 0.82 Å and this value is very similar to that found for the zero-T TS (0.83). The slope of $A(\xi)$ in the region $\xi < -1$ is only modest and the related atomic motion corresponds to the reorientation of the methyl group (decreasing the value of $r_{C-O_{Al}}$ with increasing ξ) and to a shift of the Ag^+ cation. The rapid variation of $A(\xi)$ occurring at $\xi > -1$ is related to bond breaking (C-I) and bond formation (C-O_{Al}) events.

As mentioned in Sec. 3.2, a typical reactant configuration observed in MD (R2') is not identical with the zero-temperature ground-state configuration of reactant (see Fig. 9(R2)). Configurations similar to the state R2 lie on the transformation path sampled by our blue moon ensemble simulations ($\xi =\sim -2.3$) and we were therefore able to determine the free-energy difference $\Delta A_{R2'\rightarrow R2}$, which is ∼8 kJ/mol (see Fig. 10).

The computed free-energy of activation is ∼121 kJ/mol and this value can be partitioned into internal energy and entropy contributions as follows: $\Delta U^{\ddagger}$=107 kJ/mol and $\Delta S^{\ddagger}$=−39

J/mol/K. We note that $\Delta U^{\ddagger}$ is $\sim$29 kJ/mol lower compared to our zero-T estimate (see Sec. 3.1) and, as discussed in Sec. 3.2, a part of this difference can be attributed to the potential energy difference between the finite- and zero-temperature ground states R2' and R2 ($\sim$11 kJ/mol). The negative value of $\Delta S^{\ddagger}$ is probably related to the hardening of some low-frequency vibrations (e.g. those involving Ag and I atoms) when shifting from the reactant to the transition state. Indeed, a simple static harmonic approximation to the transition state theory[53] also predicts a large negative value of $\Delta S^{\ddagger}$ (-63 J/mol/K).

The product configuration was sampled in MD run with the same setting as we used for the reactant (see Sec. 3.2). The shape of the relatively broad distribution $P(\xi)$ (see Fig. S6 in the Supporting Information[49]) reflects an increased mobility of the neutral fragment AgI formed in the course of reaction. The computed free-energy of reaction is 70 kJ/mol, and we obtained the same value also for the internal energy of reaction. This result is very different from our zero-T value ($\Delta_r E$ =94 kJ/mol) which is in part due to the potential energy difference between the zero- and finite-temperature ground-states. At a first sight, the positive value of the free-energy of dissociation might look paradoxical because spontaneous dissociation of iodomethane is observed in experiment[12] when adsorbed on Ag-exchanged zeolites. An important point to note is that a single AgI unit formed in the reaction discussed insofar is not the final product of dissociation: as we shall show in Sec. 3.4, multiple AgI units combine spontaneously to form clusters and the energy released in such a process indeed shifts the equilibrium towards dissociated state.

The free-energy profile for the reaction involving two reactant molecules per active site (see Fig. 10(b)) exhibits very similar features to that for the case with one CH_3I: the region with a modest slope ($\xi < -1$) corresponding to atomic motions that do not alter the bonding situation is followed by the region with more rapid variation of $A(\xi)$ associated with bond breaking and forming events. Due to the increased flexibility of the corresponding adsorption complex (see Sec. 3.2), the distribution of the values of ξ in the reactant state is rather broad (see Fig. S7 in the Supporting Information[49]). We chose the state ξ=-2.54 Å as a starting

point for the thermodynamic integration of free-energy gradients. The free-energy transition state is identified as ξ=0.87 Å and this value is similar to both the zero-T result (0.87 Å) and the result for the reaction involving one reactant molecule (0.82 Å). Given the increased mobility of adsorption complex, it is surprising that the computed free-energy of activation ($\Delta A^{\ddagger}$=119 kJ/mol) is very similar to that for the reaction with one CH_3I, in which the reactant is more tightly bound to the zeolite. Importantly, however, the partitioning of $\Delta A^{\ddagger}$ is distinctly different: $\Delta U^{\ddagger}$=113 kJ/mol and $\Delta S^{\ddagger}$=−16 J/mol/K (to be compared with $\Delta U^{\ddagger}$= 107 kJ/mol and $\Delta S^{\ddagger}$=−39 J/mol/K). A reduced entropy of activation is predicted also by a simple static harmonic approach:[53] $\Delta S^{\ddagger}$ decreases in absolute value from −63 J/mol/K for the reaction involving one CH_3I molecule to −36 J/mol/K for the reaction with two adsorbate molecules.

A separate MD run was performed also for the product configuration of the reaction involving two reactant molecules. In the product state, the orientation of the neutral IAg-I-CH_3 fragment formed in the reaction is approximately parallel with the main channel (see Fig. S4 in the Supporting Information[49]). The IAg-I-CH_3 species is partly immobilized due to weak interactions between the methyl group and the zeolite framework, and between Ag and methoxy group attached to zeolite. For that reason, the distribution $P(\xi)$ is significantly narrower than that computed for the reaction with one CH_3I. Similar to the case of reaction with a single CH_3I, the internal and free energies of reaction take almost identical values of 75 kJ/mol, which are higher then our zero-T result of 62 kJ/mol (Sec. 3.1).

3.4 Formation of AgI clusters in MOR

The nature of AgI, which is the observed product of conversion of iodomethane and iodine species in metal-exchanged zeolites, has been thoroughly investigated in experiment[8,14,16–18] and the measured data, such as the size, location, and geometry of the $(AgI)_n$ clusters, represent important pieces of information about the faith of the iodine species upon their adsorption. Importantly, the structure of these species and the strength of their interaction

with the host material are crucial for effective iodine trapping. We have already shown how the neutral and relatively mobile species AgI is formed upon CH_3I dissociation and in this section we shall investigate how these species combine together to form clusters and we shall also analyse their structure and energetics.

3.4.1 Structure of $(AgI)_n$ clusters

A standard MD with initial configuration containing the product of the CH_3I dissociation (see Sec. 3.1) and one extra AgI located in the main channel was performed. The lenght of the computed MD trajectory was 100 ps and the simulation temperature was set to 373 K. Note that the same setting was used in all MD simulations discussed in this section. In the initial configuration, the two AgI fragments were separated by a distance of ∼5 Å. After a relatively short period of time (∼7 ps) the fragments combined together and formed a stable two-dimensional object $(AgI)_2$. For the sake of comparison, we relaxed this configuration in a gas-phase and we found that the resulting structure (see Fig. 11(b)) is perfectly planar (symmetry D_{2h}) with all Ag-I bonds being equivalent. Compared to the relaxed monomer AgI (Fig. 11(a)), the Ag-I distance is longer by ∼0.19 Å. The geometry of the relaxed structure is in a good agreement with the $(AgI)_2$ structure reported in previous theoretical work based on DFT.[54] The finite temperature structure formed in MOR is only slightly perturbed compared to the relaxed cluster. As expected, the thermal effect led to a slight elongation of average bond lengths: the Ag-I distances increased from 2.75 Å to 2.80 Å, and the Ag-Ag separation increased from 2.78 Å to 2.95 Å. A slight decrease of the average I-I distance (from 4.74 Å to 4.70 Å) is caused by the thermal oscillations breaking the planarity of clusters. A visual inspection reveals that the $(AgI)_2$ in MOR occasionally forms also more open structures (formed when some of the Ag-I bonds is broken) that are, however, only short-living and occur only infrequently at the temperature under consideration.

Upon adding one more AgI fragment to the main channel of MOR with $(AgI)_2$, formation of a trimer $(AgI)_3$ is observed. The relaxed gas-phase structure of this compound (shown

in Fig. 11(c)) is again perfectly planar with the symmetry D_{3h}. Compared to the relaxed cluster $(AgI)_2$, the Ag-I distances are shortened by 0.09 Å while the Ag-Ag distances are elongated by 0.37 Å. The geometry of the relaxed $(AgI)_3$ and the trends observed within the series of the clusters $(AgI)_n$ are in good agreement with results reported in the previous theoretical work.[54] The $(AgI)_3$ cluster formed in MOR during the MD simulation is similar to the relaxed structure and it can be considered as quasi-planar. As in the case of dimer, the thermal effect led to a very modest elongation of the nearest-neighbour Ag-I and Ag-Ag distances (0.03 Å and 0.05 Å, respectively) while the average nearest-neighbour I-I distances remained the same as in the relaxed gas-phase cluster (5.29 Å).

Finally, a cluster $(AgI)_4$ has been prepared using the same simulation protocol as in the case of dimer and trimer and its structure is very different from the cubic cluster proposed in the experimental work of Kodaira et al.,[16] in which formation of AgI clusters in sodalite cage of zeolite LTA was studied. The tetramer identified in this work is the first member of the $(AgI)_n$ series with a truly three-dimensional structure. The relaxed gas-phase cluster (symmetry D_{2d}) is shown in Fig. 12 and we note that the same structure has been identified in the previous theoretical work[55] as the ground-state configuration of $(AgI)_4$ in the gas-phase. Notably, the cubic structure (symmetry T_d) similar to that proposed by Kodaira et al.[16] was found to be ∼45 kJ/mol higher in energy.[55] In our gas-phase cluster, all silver atoms are co-planar and occupy corners of a perfect square with a side of length of 3.24 Å. The iodine atoms are distributed in such a way that the lengths of the shortest Ag-I and I-I distances (2.64 Å and 5.28 Å, respectively) are almost identical to those in the relaxed trimer. The I-I separation for pairs of atoms which do not share a common Ag is 6.48 Å (see Fig. 12(b)). The thermal motion in the confining environment of the main channel of MOR breaks the symmetry more significantly than in the case of smaller clusters. This is particularly evident on the arrangement of the Ag atoms, which is now rectangular rather than square-like, with the longer side being oriented parallel with the channel (see Fig. S5 in the Supporting Information[49]). The average values of two shortest Ag-Ag separations

are 2.92 Å and 4.12 Å. The average length of the Ag-I bond is 2.68 Å, which is similar to the value found in the relaxed structure and in the finite-temperature structures of smaller clusters. Due to the reduced symmetry, the average I-I distances changed as follows: the pairs of I atoms bound to the same Ag are separated by 5.19 Å (i.e. 0.09 Å less compared to the relaxed structure), while the distances between the pairs which do not share a common Ag atom are 4.44 Å and 7.00 Å (to be compared with the zero-T value of 6.48 Å). Hence the shortest I-I distance found in the $(AgI)_4$ cluster is even shorter than that identified in other two clusters considered here and this shortening is possible only due to the non-planar arrangement of $(AgI)_4$. We note that the size of the tetramer identified in this work is close to the size of the $(AgI)_n$ clusters observed in experiment.[14]

An experimental information about the structure of $(AgI)_n$ in MOR is available from the measured radial distribution functions obtained in X-ray scattering experiments.[8,14] In Fig. 13 we compare RDF determined for all pairs of Ag and I atoms in $(AgI)_n$ in MOR using our MD data with the experimental result.[8] As evident, already the RDF computed for the dimer reproduces rather well the first measured feature, which is a slightly asymmetric peak centred at ∼2.8 Å. Our calculations show that this peak is actually a superposition of two contributions from the Ag-I and Ag-Ag pairs. As the number of AgI units increases, the position of the first peak is shifted slightly towards shorter distances (∼2.65 Å in the case of $(AgI)_4$) and this trend is in line with the shortening of the average Ag-I distances with the cluster size discussed above. In the case of trimer, the two features forming the first peak are well resolved (∼2.7 Å and ∼3.2 Å for Ag-I and Ag-Ag, respectively).

The second major feature observed in the measured RDF is a broad band centred at ∼4.4 Å and spread over the interval between ∼3.6 Å to ∼5.4 Å (see Fig. 13). Not surprisingly, different clusters contribute to this band differently. In the case of the dimer, only a narrow peak due to the I-I pair positioned at ∼4.7 Å overlaps with the measured band. Similarly, the calculations performed for the $(AgI)_3$ predict only a narrow peak at ∼5.3 Å due to the nearest neighbour I-I distances mixed with the contribution of the small wider band from

the next-nearest neighbour Ag-I distances. The most complex situation is found for the tetramer. Here, in accord with experiment, we observe formation of a wide band cantered at ∼4.4 Å and spread over the interval between ∼3.5 Å and ∼4.8 Å and this feature is due to the contributions from the nearest neighbour I-I and the next-nearest neighbour Ag-Ag and Ag-I distances. Furthermore, the next-nearest I-I distances form a narrower peak centered at ∼5.2 Å and spread over the interval between ∼4.8 Å and ∼5.6 Å. Obviously, both peaks overlap with the experimentally measured band. Although the relative heights of these two features differ from experiment, our cluster $(AgI)_4$ represents the smallest model that can be used to reproduce the measured RDF. One can expect that a further redistribution of relative heigths of features forming the second peak observed in experiment will occur if the size of cluster is increased. We note, however, that the size of tetramer is already close to the size of clusters observed in experiment (∼7 Å). We also remark that clusters of different size can be expected to coexist in reality and the measured RDF should be therefore considered as a superposition of contributions from several different structures.

3.4.2 Energetics of $(AgI)_n$ clusters

Energy of formation of $(AgI)_n$ clusters represents an important contribution to the overall energetics of the CH_3I adsorption in Ag-MOR. We have shown in Sec. 3.3 that the free-energy of dissociation is positive (70 kJ/mol). Hence, in order to shift equilibrium towards the dissociated CH_3I (as observed in experiment), free-energy of formation must take a sufficiently large negative value so that its sum with the free energy of dissociation is negative. Unfortunately, the calculations of free-energies of formation would be extremely time-consuming as they would require the use of a very large structural model allowing for sufficiently large separation of the AgI units to prevent their spontaneous reaction. We therefore analyse only the more easily accessible internal energy, which is certainly the dominant contribution to the free-energy of formation.

We start our analysis with energetics of the gas-phase clusters. Using the energies of

structures obtained in atomic relaxations, the contribution of a single AgI unit to the zero-temperature energy can be determined using eq. 2. The computed values of energy of formation ($\Delta_f E$) increase with n as follows: -90 kJ/mol (n=2), -147 kJ/mol (n=3), and -154 kJ/mol (n=4). This trend is not surprising: it indicates that formation of clusters from isolated AgI units is energetically favourable and the energy gained by inserting an additional AgI decreases with n. In the n$\rightarrow \infty$ limit, the value of $\Delta_f E$ should reach the bulk limit which is, according to our calculations, -212 kJ/mol for the low temperature phase β-AgI. A similar convergence of cluster energies towards the bulk limit is reported also in the previous theoretical work of Krawczyk et al.[56] Somewhat lower absolute values of $\Delta_f E$ for AgI clusters have been determined in previous DFT calculations performed at the B3LYP level:[54,55] -74 kJ/mol (n=2), -116 kJ/mol (n=3), and -133 kJ/mol (n=4). Our value computed for the trimer (-147 kJ/mol) compares reasonably well with enthalpy determined for this structure experimentally at T=298 K[57] (-135 kJ/mol).

The internal energy of formation of gas-phase clusters ($\Delta_f U_{gas}$) at T=373 K has been determined using MD simulations. The computed values obtained using eq. 4 differ only moderately from our zero-temperature results but, as expected, the difference increases with the number of AgI units in the cluster: -90 kJ/mol (n=2), -144 kJ/mol (n=3), and -146 kJ/mol (n=4). Compared to these values, the internal energy of formation of $(AgI)_n$ in the interior of mordenite ($\Delta_f U_{zeo}$) computed using eq. 5 is systematically higher (-46 kJ/mol (n=2), -77 kJ/mol (n=3), and -79 kJ/mol (n=4)), which is due to the fact that, that the interaction energy between the clusters and zeolite expressed per AgI unit decreases with the cluster size (*vide infra*). Hence the sum of internal energy of dissociation (70 kJ/mol) and cluster formation takes a negative value for the cluster containing more than two AgI units.

Finally, we determined internal energy of interaction between clusters and mordenite using eq. 3. According to our calculations, this quantity tends to increase with n as follows: -105 kJ/mol (n=1), -122 kJ/mol (n=2), -114 kJ/mol (n=3), and -150 kJ/mol (n=4).

The exception in the trend occurring for n=3 is likely due to the sterical reasons because the large quasi-planar and quasi-triangular structure of $(AgI)_3$ (see Fig. 11(c)) is more difficult to get oriented in an optimal way with respect to the zeolite framework than the smaller clusters AgI and $(AgI)_2$, or the cluster $(AgI)_4$ with a more compact 3D structure.

4 Conclusions

Dissociative adsorption of iodomethane on Ag-MOR has been studied by means of ab-initio molecular dynamics and zero-temperature structural relaxations. Our zero-temperature analysis indicates that the reaction proceeds at the highest rate via a simple one-step mechanism involving the Ag^+ sites. The co-adsorption of two CH_3I molecules on the same active site leads to a significant decrease (by 38 kJ/mol) of the zero-temperature activation energy. In contrast, an unfavourable zero-temperature reaction energetics for the mechanism involving the Brønsted acid sites suggests that this mechanism probably does not play a significant role in the CH_3I dissociation.

The finite-temperature effect on the interaction between adsorbate and the adsorption site Ag^+ has been investigated using MD simulations. It has been shown that binding of the Ag^+ site to zeolite is significantly reduced upon interaction with the CH_3I molecule. Consequently, the adsorption complex Ag-ICH_3 is relatively mobile although still fixed via one strong bond to one O atom next to the framework Al. Adsorption of one additional molecule leads to a further weakening of the interaction between the Ag^+ site and the zeolite framework causing a very significant increase in mobility of the corresponding adsorption complex. As the complexes with three CH_3I molecules are found to be unstable, we conclude that the Ag^+ site is fully saturated upon binding two adsorbate molecules. This result is consistent with the experimental work of Chebbi et al.[50] who found that the values of the I/Ag ratio in various Ag-exchanged zeolites saturated by adsorption of CH_3I are significantly lower than 2 (the highest value of I/Ag=1.58 is reported for the zeolite X). Internal energies

of adsorption computed using MD are −117 kJ/mol and −99 kJ/mol for the complexes with one and two adsorbate molecules, respectively. These numerical results are markedly lower in absolute value than the corresponding zero-T estimates (−145 and −109 kJ/mol) which is mainly due to the fact that the zero-T calculations deal only with the energetically most favourable configurations while the finite-T calculations average over ensemble of all configurations accessible at the given temperature.

Detailed finite-temperature analysis of reaction energetics has been performed using thermodynamic intergration of free-energy gradients. For the reaction with a single reactant molecule, both the computed reaction barrier (121 kJ/mol) and the free-energy of reaction (70 kJ/mol) decrease significantly compared to the zero-T results (136 kJ/mol and 94 kJ/mol, respectively) and a part of this difference (∼8 kJ/mol) has been found to be due to the change of the ground-state configuration of reactant when increasing temperature. Partitioning of free-energy into internal energy and entropy contributions allowed us to identify the terms $\Delta U^{\ddagger}$= 107 kJ/mol, $\Delta S^{\ddagger}$=−39 J/mol/K, and $\Delta_r U$ = 70 kJ/mol.

Adsorption of additional CH_3I molecule has only a minor effect on the free-energetics of reaction: the computed values $\Delta A^{\ddagger}$=119 kJ/mol and $\Delta_r A$ = 75 kJ/mol are very close to the values determined for the reaction with a single CH_3I. Although the free-energy barrier is rather similar to the zero-T result ($\Delta E^{\ddagger}$= 114 kJ/mol), the trend drawn from the zero-T calculations is distinctly different as they predict a significant decrease of reaction barrier upon adsorption of the second molecule. The partitioning of free-energy barrier reveals that this variant of reaction is linked with a much smaller change in entropy ($\Delta S^{\ddagger}$=−16 J/mol/K) compared to the reaction with a single CH_3I. As in the case of the reaction with a single CH_3I, the entropy of reaction is negligible and hence $\Delta_r A$ and $\Delta_r U$ take almost identical values of ∼75 kJ/mol.

The structure and energetics of the $(AgI)_n$ clusters formed upon dissociative adsorption of CH_3I in Ag-MOR have been analysed in detail. The $(AgI)_n$ clusters are shown to be formed spontaneously upon interaction of AgI (formed as a product of dissociation of CH_3I)

with a previously created cluster $(AgI)_{n-1}$. The clusters with n=2,3 are planar and their structures in MOR are very similar to their gas-phase geometries. In contrast, the cluster $(AgI)_4$ is non-planar. While its structure in zeolite can still be related to that of the ground-state gas-phase configuration,[54,55] the deformations due to the interactions with the zeolite framework are quite significant. The length of this cluster is ∼7 Å, which is close to the value proposed experimentally as a limiting size of the $(AgI)_n$ clusters formed in MOR.[14] Importantly, the value n=4 was found also in other experimental work[10] as the most-likely number of monomers in the clusters formed in various zeolites. The structure of $(AgI)_4$ is significantly different from the cubic structure proposed in the experimental work of Kodaira et al.[16] and Heo et al.[18] in which the formation of the AgI clusters in sodalite cages of zeolites LTA and A was studied. A possible explanation of this discrepancy is that the space in the sodalite cage is much more restricted and hence it strongly affects the structure of the clusters formed inside this cavity. In contrast, one can expect that the clusters will assume structures more similar in shape to the corresponding gas-phase ground state configurations when formed in zeolites with less confining voids (such as MOR considered in this work).

The radial distribution functions computed for various clusters differ significantly and only the RDF determined for n=4 exhibits both important features of RDF observed in experiment (a sharp peak at ∼2.8 Å, and a broad band centred at ∼4.4 Å that spreads over the interval between 3.6 Å and 5.4 Å), although the agreement is not perfect. It should be noted, however, that the measured RDF averages over a distribution of various $(AgI)_n$ clusters and hence it should be considered as a superposition of contributions from many different structures.

When the individual AgI units formed upon CH_3I dissociation combine together to form the $(AgI)_n$ clusters, the internal energy of the system decreases and consequently, the equilibrium cab be eventually shifted towards the dissociated form of adsorbate. The computed internal energy of formation of the $(AgI)_n$ clusters in MOR decreases with n as follows: −46 kJ/mol (n=2), −77 kJ/mol (n=3), and −79 kJ/mol (n=4). Combined with the computed

value of internal energy of dissociation (70 kJ/mol) we find that the dissociation process becomes energetically favourable for the cluster sizes n≥3. The computed interaction energy between zeolite and clusters decreases with n as follows: −105 kJ/mol (n=1), −122 kJ/mol (n=2), −114 kJ/mol (n=3), and −150 kJ/mol (n=4) and these relatively high negative values are, together with the expected reduced mobility of larger clusters, essential for a sufficiently long stability of iodine trapped in MOR.

Altogether, this work represents a further step in our systematic investigation of iodine trapping in Ag-exchanged zeolites. It is well documented[12] that the adsorption capacity of Ag-MOR increases with the Ag^+ content. In addition to isolated Ag^+ sites, more complex forms of cationic silver can be formed when the Ag^+ content is high. In our future work we therefore plan to extend this study to include pairs of Ag^+ cations in the main channel, which have been proposed as energetically favourable adsorption sites in the recent theoretical work Chibani et al.[11] Furthermore, some important technological applications require that the iodine trapping is efficient also at wet conditions and the presence of water molecules will certainly interact with adsorption sites and with the adsorbate molecules. In our future work we plan to investigate also this important aspect of iodine trapping.

Acknowledgments

This work has been supported by the Slovak Research and Development Agency under the contract No. APVV-15-0105, and by the French State under the program "Investissements dAvenir MiRE managed by the ANR under grant agreement ANR-11-RSNR-0013-01. TB is thankful to University of Lorraine for invited professorship in the academic year 2015/16. SC thanks the National Research Agency (ANR) for her postdoctoral grant. Calculations were performed using supercomputing infrastructure of Computing Center of the Slovak Academy of Sciences acquired in projects ITMS 26230120002 and 26210120002 supported by the Research and Development Operational Program funded by the ERDF. We also ac-

knowledge the PMMS (Computational Center in Metz) and GENCI-CCRT/CINES (Grants No. 2017-085106 and No. 2017- A0010810169) for providing us with the HPC resources.

A Free-energy calculations

Let us assume that a reversible transformation between two stable states of the same system under NVT conditions can be realized by varying the value of a single geometric parameter (reaction coordinate) $\xi = \xi(\boldsymbol{r})$ that is a function of Cartesian coordinates $\boldsymbol{r}$. The two stable states - reactant (R) and product (P) - are separated by a barrier which reaches its maximum at the point $\xi(\boldsymbol{r}) = \xi^*$. For simplicity, let us assume that all configurations of the state R fulfil the condition $\xi \leq \xi^*$, and a complementary condition $\xi \geq \xi^*$ defines the state P. Within the Eyring's transition state theory,[58] the rate constant for an activated process writes:[59]

$$k_{R\to P} = \frac{\langle \dot{\xi}\theta(\dot{\xi})\delta(\xi^* - \xi(0))\rangle}{\langle \theta(\xi^* - \xi)\rangle}, \tag{7}$$

where $\dot{\xi}$ is the generalized velocity associated with the coordinate ξ, θ is the Heaviside step function, $\xi(0)$ is the value of reaction coordinate at the time t=0, and the angular brackets represent the thermodynamic averages. This formula can be rewritten as follows:

$$k_{R\to P} = \frac{\langle|\dot{\xi^*}|\rangle}{2} P(\xi_{ref,R}) \exp\left(-\frac{\Delta A_{\xi_{ref,R}\ \to\xi^*}}{k_B\, T}\right), \tag{8}$$

where $\xi_{ref,R}$ is a reference point chosen from the values of ξ characteristic for the reactant state, $P(\xi_{ref,R}) = \frac{\langle\delta(\xi_{ref,R}-\xi)\rangle}{\langle\Theta(\xi^*-\xi)\rangle}$ is the probability density of $\xi_{ref,R}$ within the ensemble of reactant configurations, $\dot{\xi^*}$ is the velocity associated with reaction coordinate for configurations at the transition state, and $\Delta A_{\xi_{ref,R}\ \to\xi^*} = -k_B T ln\left[\frac{P(\xi^*)}{P(\xi_{ref,R})}\right]$ is the reversible work needed to shift the reaction coordinate from the value $\xi_{ref,R}$ to ξ^*. Note that while the value of $\xi_{ref,R}$ can be chosen arbitrarily, it is advantageous to define $\xi_{ref,R}$ so that the density $P(\xi_{ref,R})$ can be be determined using a straightforward MD. In this work we choose $\xi_{ref,R}$ to

be close to expected maximum of $P(\xi_R)$, see Sec.SIV in the Supporting Information.[49] The term $\Delta A_{\xi_{ref,R} \rightarrow \xi^*}$ can be computed by any method designed for calculation of free-energy of activated processes, such as umbrella sampling,[60] metadynamics,[61] or steered dynamics;[62] as discussed below, in this work we choose the blue moon ensemble method.[38] Finally, the generalized velocity is determined numerically using the following equation:

$$\dot{\xi} = \sum_{i=1}^{N} \sum_{\mu=x,y,z} \frac{\partial \xi}{\partial \boldsymbol{r}_{i,\mu}} \dot{\boldsymbol{r}}_{i,\mu}, \tag{9}$$

where summations are over all atoms comprising the system (N) and over all components of Cartesian coordinates. The Cartesian velocity components $\dot{\boldsymbol{r}}_{i,\mu}$ are random-generated from the Maxwell-Boltzmann distribution. In practice, we first identify the value of ξ^* which corresponds to the point at the top of the free-energy barrier (with vanishing free-energy gradient *vide infra*) separating reactant and product. Next we generate an ensemble of configurations with $\xi = \xi^*$ using constrained MD, and finally we use eq. 9 to compute $|\dot{\xi^*}|$ for 1000 configurations and 500 random values of $\dot{r}_{i,\mu}$. In order to obtain unconstrained average, the following formula is used:

$$\langle |\dot{\xi^*}| \rangle = \frac{\langle Z^{-1/2} |\dot{\xi}| \rangle_{\xi^*}}{\langle Z^{-1/2} \rangle_{\xi^*}}, \tag{10}$$

where $\langle \cdots \rangle_{\xi^*}$ stands for constrained average, and Z is defined as follows:

$$Z = \sum_{i=1}^{N} \frac{1}{m_i} \sum_{\mu=x,y,z} \left(\frac{\partial \xi}{\partial \boldsymbol{r}_{i,\mu}} \right)^2, \tag{11}$$

with m_i being the mass of atom i.

By comparing eq. 8 with the Eyring-Polanyi equation:[58]

$$k_{R \rightarrow P} = \frac{k_B T}{h} \exp\left(-\frac{\Delta A^{\ddagger}}{k_B T} \right), \tag{12}$$

the following relation between the phenomenological free-energy of activation ($\Delta A^{\ddagger}$) and reversible work $\Delta A_{\xi_A \rightarrow \xi^*}$ can be obtained:

$$\Delta A^{\ddagger} = \Delta A_{\xi_{ref,R} \rightarrow \xi^*} - k_B T \ln \left(\frac{h}{k_B T} \frac{\langle |\dot{\xi^*}(0)| \rangle}{2} P(\xi_{ref,R}) \right) \tag{13}$$

Making use of expression for the constant of equilibrium between the states R and P:

$$K_{R \rightarrow P} = \frac{k_{R \rightarrow P}}{k_{P \rightarrow R}}, \tag{14}$$

and employing eq. 8 and its analogue for $k_{P \rightarrow R}$, we find the following expression for the free-energy of reaction ($\Delta A_{R \rightarrow P} = -k_B T \ln (K_{R \rightarrow P})$):

$$\Delta A_{R \rightarrow P} = \Delta A_{\xi_{ref,R} \rightarrow \xi_{ref,P}} - k_B T \ln \left(\frac{P(\xi_{ref,R})}{P(\xi_{ref,P})} \right), \tag{15}$$

where $\xi_{ref,P}$ is the reference point for the product configurations, $P(\xi_{ref,P})$ is its probability density among the product configurations, and $\Delta A_{\xi_{ref,R} \rightarrow \xi_{ref,P}}$ is the reversible work needed to shift the value of $\xi(\boldsymbol{r})$ from $\xi_{ref,R}$ to $\xi_{ref,P}$. The latter term is again computed using the blue moon ensemble method discussed below.

The blue moon ensemble method[38] is based on integration of free-energy gradients along the reaction path connecting two states A and B:

$$\Delta A_{A \rightarrow B} = \int_{\xi_A}^{\xi_B} \left(\frac{\partial A}{\partial \xi} \right)_{\xi^*} d\xi. \tag{16}$$

The free-energy gradients are determined using constrained MD simulations using the following formula:[38,63–65]

$$\left(\frac{\partial A}{\partial \xi} \right)_{\xi^*} = \frac{1}{\langle Z^{-1/2} \rangle_{\xi^*}} \langle Z^{-1/2} [-\lambda + k_B T Z^{-1} \sum_{i=1}^{N} \sum_{\mu=x,y,z} \frac{1}{m_i} \frac{\partial \xi}{\partial \boldsymbol{r}_{i,\mu}} \frac{\partial Z}{\partial r_{\mu,i}}] \rangle_{\xi^*}, \tag{17}$$

where $\langle ... \rangle_{\xi^*}$ stands for the statistical average of the quantity enclosed in angular parenthe-

ses computed for a constrained ensemble, λ is a Lagrange multiplier associated with the parameter ξ used in the SHAKE algorithm[66] and Z is the mass metric tensor defined in eq. 11.

B Free-energy partitioning

We partition the free-energy into internal energy and entropy contribution using the well known relation:

$$A = U - TS \tag{18}$$

In calculation of reaction energetics, the term $\Delta_r A \equiv \Delta A_{R\to P}$ is computed as described in Appendix A. The internal energy of reaction $\Delta_r U \equiv \Delta U_{R\to P}$ is obtained using average total energies from MD runs for reactant and product as follows:

$$\Delta_r U = \langle E_P \rangle - \langle E_R \rangle, \tag{19}$$

where E_P and E_R are the total energies of product and reactant, respectively. Having computed $\Delta_r A$ and $\Delta_r U$, the entropy of reaction is determined using eq. 18.

The partitioning of $\Delta A^{\ddagger}$ requires a slightly greater effort. Having determined the free-energy transition state (see Appendix A), constrained MD with $\xi = \xi^*$ is performed and the average total energy of transition state is obtained using the following formula:[38]

$$\langle E_{TS} \rangle = \frac{\langle Z^{-1/2} E_{TS} \rangle_{\xi^*}}{\langle Z^{-1/2} \rangle_{\xi^*}}, \tag{20}$$

with Z defined in eq. 11. The internal energy of activation is then computed as follows:

$$\Delta U^{\ddagger} = \langle E_{TS} \rangle - \langle E_R \rangle \tag{21}$$

and $\Delta S^{\ddagger}$ is obtained using eq. 18.

References

(1) Goldsmith, J.; Grossman, C.; Morton, W.; Nussbaum, R.; Kordysh, E.; Ouastel, M.; Sobel, R.; Nussbaum, F. *Environ. Health Perspect.* **1999**, *107*, 303–308.

(2) Grossman, C. M.; Nussbaum, R. H.; Nussbaum, F. D. *Arch. Environ. Health* **2003**, *58*, 267–274.

(3) Hidaka, A.; Yokoyama, H. *Journal of Nuclear Science and Technology* **2017**, *54*, 819–829.

(4) Clement, B.; Cantrel, L.; Ducros, G.; Funke, F.; Herranz, L.; Rydl, A.; Weber, G.; Wren, C. *OCDE Report*; NEA/CSNI/R(2007)1, 2007; p 11.

(5) Belapurkar, A.; Rao, K. A.; Gupta, N.; Iyer, R. *Surf. Technol.* **1984**, *21*, 263 – 272.

(6) Murray, D. K.; Chang, J. W.; Haw, J. F. *J. Am. Chem. Soc.* **1993**, *115*, 4732–4741.

(7) Choi, B.; Park, G.; Kim, J.; Lee, J.; Ryu, S. *Adsorption* **2001**, *7*, 91–103.

(8) Nenoff, T. M.; Rodriguez, M. A.; Soelberg, N. R.; Chapman, K. W. *Microporous Mesoporous Mater.* **2014**, *200*, 297–303.

(9) Riley, B. J.; Vienna, J. D.; Strachan, D. M.; McCloy, J. S.; Jerden, J. L., Jr. *J. Nucl. Mater.* **2016**, *470*, 307–32.

(10) Chebbi, M.; Azambre, B.; Cantrel, L.; Koch, A. *J. Phys. Chem. C* **2016**, *120*, 18694–18706.

(11) Chibani, S.; Chebbi, M.; Lebègue, S.; Cantrel, L.; Badawi, M. *Phys. Chem. Chem. Phys.* **2016**, *18*, 25574–25581.

(12) Chebbi, M.; Azambre, B.; Cantrel, L.; Huv, M.; Albiol, T. *Microporous and Mesoporous Mater.* **2017**, *244*, 137 – 150.

(13) Karhu, A. *Report VTT Energy, Finland*; NKS, 1999; pp 11–13.

(14) Chapman, K. W.; Chupas, P. J.; Nenoff, T. M. *J. Am. Chem. Soc.* **2010**, *132*, 8897.

(15) Chibani, S.; Chebbi, M.; Lebègue, S.; Bucko, T.; Badawi, M. *J. Chem. Phys.* **2016**, *144*.

(16) Kodaira, T.; Ikeda, T.; Takeo, H. *Eur. Phys. J. D* **1999**, *9*, 601–604.

(17) Kodaira, T.; Ikeda, T.; Takeo, H. *Chem. Phys. Lett.* **1999**, *300*, 499–503.

(18) Heo, N.; Kim, H.; Lim, W.; Seff, K. *J. Phys. Chem. B* **2004**, *108*, 3168–3173.

(19) Kresse, G.; Hafner, J. *Phys. Rev. B* **1993**, *48*, 13115.

(20) Kresse, G.; Hafner, J. *Phys. Rev. B* **1994**, *49*, 14251.

(21) Kresse, G.; Furthmüller, J. *Computat. Mater. Sci.* **1996**, *6*, 15.

(22) Kresse, G.; Furthmüller, J. *Phys. Rev. B* **1996**, *54*, 11169.

(23) Blöchl, P. *Phys. Rev. B* **1994**, *50*, 17953.

(24) Kresse, G.; Joubert, D. *Phys. Rev. B* **1999**, *59*, 1758.

(25) Perdew, J. P.; Burke, K.; Ernzerhof, M. *Phys. Rev. Lett.* **1996**, *77*, 3865–3868.

(26) Grimme, S. *J. Comp. Chem.* **2006**, *27*, 1787.

(27) Bucko, T.; Hafner, J.; Lebègue, S.; Angyan, J. G. *J. Phys. Chem. A* **2010**, *114*, 11814–11824.

(28) Goeltl, F.; Grueneis, A.; Bucko, T.; Hafner, J. *J. Chem. Phys.* **2012**, *137*, 114111.

(29) Henkelman, G.; Jónsson, H. *J. Chem. Phys.* **1999**, *111*, 7010.

(30) Heyden, A.; Bell, A.; Keil, F. *J. Chem. Phys.* **2005**, *123*, 224101.

(31) Fukui, K. *J. Phys. Chem.* **1970**, *74*, 4161.

(32) Fukui, K. *Accounts of Chemical Research* **1981**, *14*, 363.

(33) Hratchian, H.; Schlegel, H. *J. Phys. Chem. A* **2002**, *106*, 165.

(34) Press, W. H.; Flannery, B. P.; Teukolsky, S. A.; Vetterling, W. T. *Numerical Recipes in FORTRAN 77: The Art of Scientific Computing (v. 1)*, 2nd ed.; Cambridge University Press, 1992; p 413.

(35) Nosé, S. *J. Chem. Phys.* **1984**, *81*, 511.

(36) Hoover, W. *Phys. Rev. A* **1985**, *31*, 1695.

(37) Schwarz, M.; Hache, G.; von der Hardt, P. *Nucl. Eng. Des.* **1999**, *187*, 47–69.

(38) Carter, E.; Ciccotti, G.; Hynes, J.; Kapral, R. *Chem. Phys. Lett.* **1989**, *156*, 472.

(39) Bucko, T. *J. Phys. Condens. Matt.* **2008**, *20*, 064211.

(40) Alberti, A.; Davoli, P.; Vezzalini, G. *Z. Kristallogr.* **1986**, *175*, 249.

(41) Mortier, W. *Compilation of extra framework sites in zeolites*; Butterworth, Guildford, 1982.

(42) Demuth, T.; Hafner, J.; Benco, L.; Toulhoat, H. *J. Phys. Chem. B* **2000**, *104*, 4593–4607.

(43) Schlner, J.; Pluth, J.; Smith, J. *Mater. Res. Bull.* **1979**, *14*, 849.

(44) Baltrusaitis, J.; Bucko, T.; Michaels, W.; Makkee, M.; Mul, G. *Appl. Catal., B* **2016**, *187*, 195–203.

(45) Bosacek, V. *J. Phys. Chem.* **1993**, *97*, 10732–10737.

(46) Mignon, P.; Geerlings, P.; Schoonheydt, R. *J. Phys. Chem. B* **2006**, *110*, 24947–24954.

(47) Bucko, T.; Lebègue, S.; Hafner, J.; Angyan, J. G. *J. Chem. Theory Comput.* **2013**, *9*, 4293–4299.

(48) Bucko, T.; Lebègue, S.; Hafner, J.; Angyan, J. G. *J. Chem. Phys.* **2014**, *141*, 034114.

(49) The Supporting Information is available free of charge on the ACS Publications website at [URL will be inserted by ACS]. Energetics of alternative dissociation mechanism, description of coordination number calculation from RDF, snapshots taken from MD, and probability distributions used in the free-energy calculations.

(50) Chebbi, M. *Thesis*; University of Lorraine, 2016; pp 180–218.

(51) Bucko, T.; Benco, L.; Hafner, J.; Angyan, J. G. *J. Catal.* **2011**, *279*, 220.

(52) Bucko, T.; Hafner, J. *J. Catal.* **2015**, *329*, 32–48.

(53) Jensen, F. *Introduction to computational chemistry*; John Wiley & Sons, Chichester, 1997; pp 296–307.

(54) Khairallah, G. N.; O'Hair, R. A. J. *Dalton Trans.* **2008**, 2956–2965.

(55) Schwerdtfeger, P.; Krawczyk, R. P.; Hammerl, A.; Brown, R. *Inorg. Chem.* **2004**, *43*, 6707–6716.

(56) Krawczyk, R. P.; Hammerl, A.; Schwerdtfeger, P. *Chem. Phys. Chem.* **2006**, *7*, 2286–2289.

(57) Binnewies, M.; Schfer, H. *Z. Anorg. Allg. Chem.* **1973**, *395*, 63–68.

(58) Atkins, P.; de Paula, J. *Atkins' physical chemistry*; Oxford university press: San Diego, 2002; pp 956–963.

(59) Frenkel, D.; Smit, B. *Understanding molecular simulation: from algorithms to applications*; Academic press: San Diego, 2002; pp 436–450.

(60) Torrie, G.; Valleau, J. *J. Comput. Phys.* **1977**, *23*, 187 – 199.

(61) Laio, A.; Parrinello, M. *Proc. Natl. Acad. Sci. U.S.A.* **2002**, *99*, 12562.

(62) Park, S.; Khalili-Araghi, F.; Tajkhorshid, E.; Schulten, K. *J. Chem. Phys.* **2003**, *119*, 3559–3566.

(63) Den Otter, W.; Briels, W. *Mol. Phys.* **2000**, *98*, 773–781.

(64) Darve, E.; Wilson, M.; Pohorille, A. *Mol. Simul.* **2002**, *28*, 113.

(65) Fleurat-Lessard, P.; Ziegler, T. *J. Chem. Phys.* **2005**, *123*, 084101.

(66) Ryckaert, J.; Ciccotti, G.; Berendsen, H. *J. Comp. Phys.* **1977**, *23*, 327.

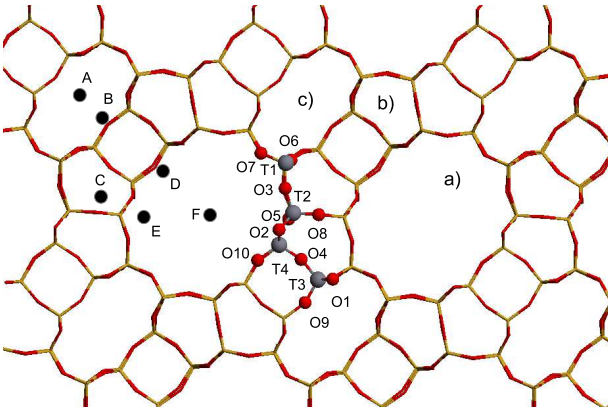

Figure 1: Crystal structure of mordenite (MOR) projected along the *c*-direction. The voids available in MOR for molecular adsorption include main channel (a), side pocket (b), and small channel (c). The labeling of the tetrahedral (T) and oxygen (O) sites of the framework follows Ref.[40] The possible locations of extra-framework cations classified by Mortier (Ref.[41]) are labeled by capital letters (A to F).

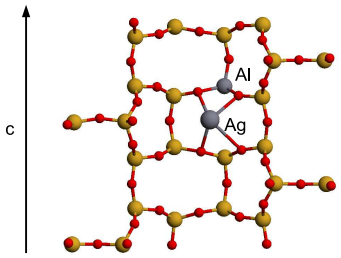

Figure 2: Structural model of Ag-MOR used in this work. The direction of lattice vector parallel with the main channel is indicated. The Al atom is in the tetrahedral position T1 and the initial location of Ag^+ corresponds to the Mortier position E (cf. Fig. 1).

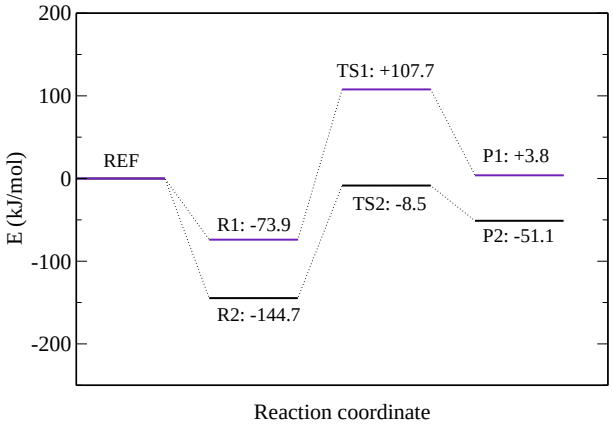

Figure 3: Reaction energy profiles for two reaction mechanisms of iodomethane dissociation over MOR: the sequence R1→TS1→P1 (mechanism I) involves Brønsted acid site (see Fig. 4), and reaction R2→TS2→P2 (mechanism II) involves the Ag^+ site and leads to the formation of methoxy species on the Al-O-Si bridge of zeolite (see Fig. 5). Zero on the energy axis (state REF) corresponds to the sum of energies of non-interacting gas phase molecule CH_3I and of clean H-MOR (mechanism I) or Ag-MOR (mechanism II).

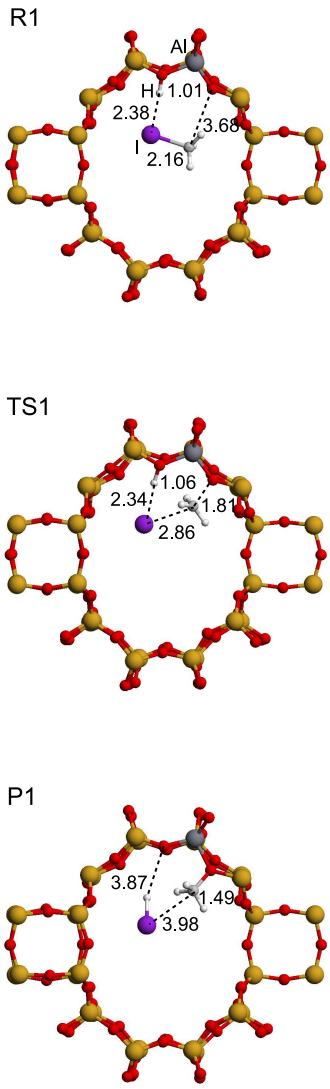

Figure 4: Configurations corresponding to stationary points on the potential energy surface for the CH_3I dissociation via mechanism I: reactant (R1), transition state (TS1), and product (P1). Selected interatomic distances are in Å.

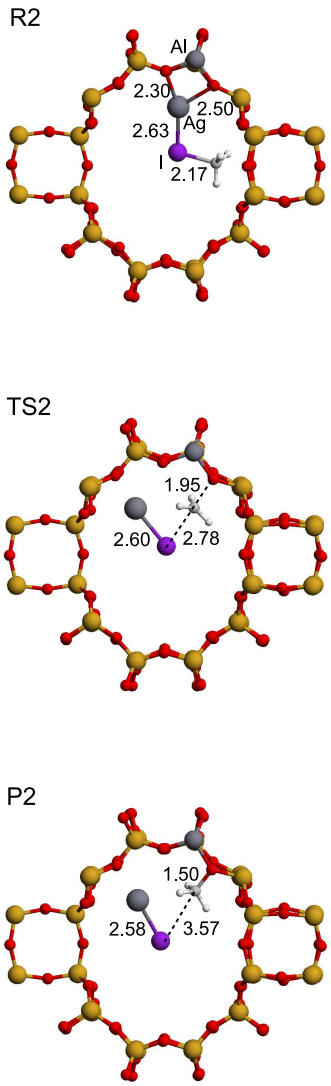

Figure 5: Configurations corresponding to stationary points on the potential energy surface for the CH_3I dissociation via mechanism II: reactant (R2), transition state (TS2), and product (P2). Selected interatomic distances are in Å.

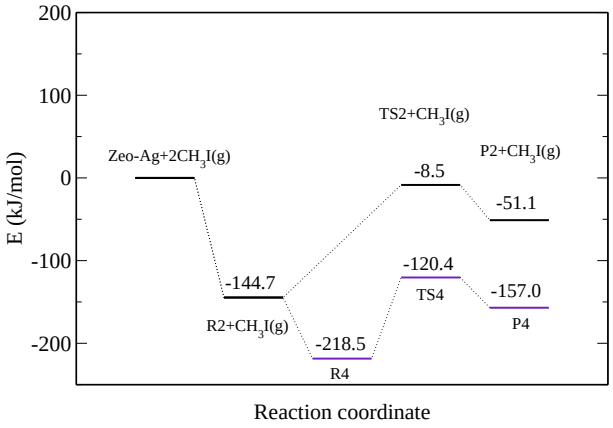

Figure 6: Variation of energy profiles for the iodomethane dissociation over Ag-MOR with saturation of the Ag^+ site: one reactant molecule per Ag^+ (R2→TS2→P2) and two reactant molecules per Ag^+ (R4→TS4→P4). The zero on the energy axis corresponds to the sum of energies of two non-interacting gas phase molecules CH_3I and of clean substrate. The geometries of related stationary states are shown in Fig. 5 and Fig. 7.

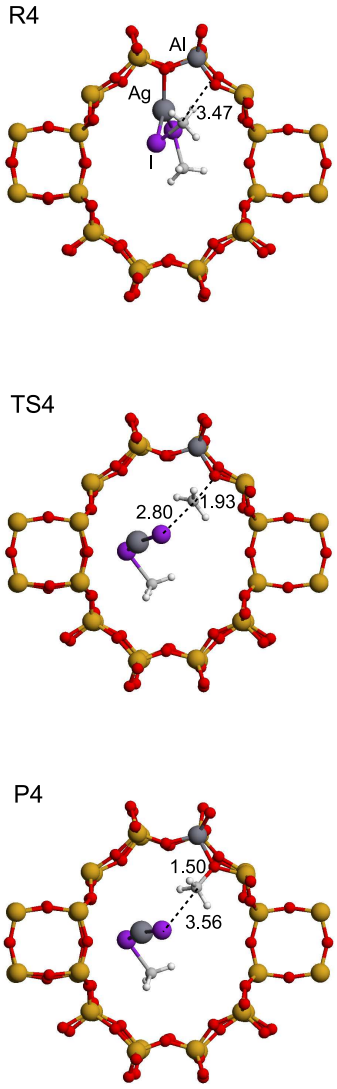

Figure 7: Configurations corresponding to stationary points on the potential energy surface for the iodomethane dissociation starting from adsorption complex with two reactant molecules on a single Ag^+ site: reactant (R4), transition state (TS4), and product (P4). Selected interatomic distances are in Å.

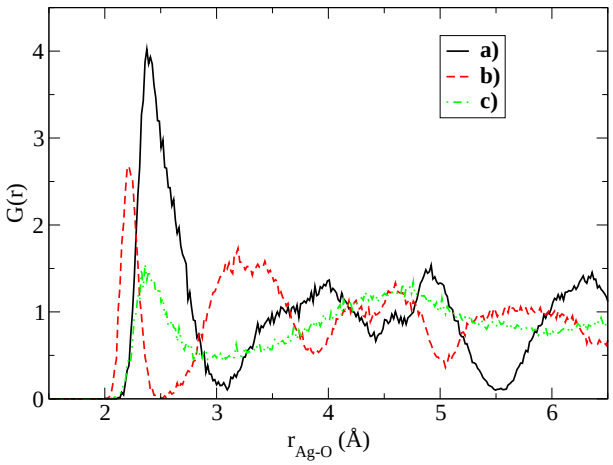

Figure 8: Radial distribution function (G(r)) for the Ag-O pairs in (a) clean Ag-MOR, (b) adsorption complex formed by one CH_3I molecule attached to the cation Ag^+, and (c) adsorption complex formed by two CH_3I molecule on the Ag^+ site.

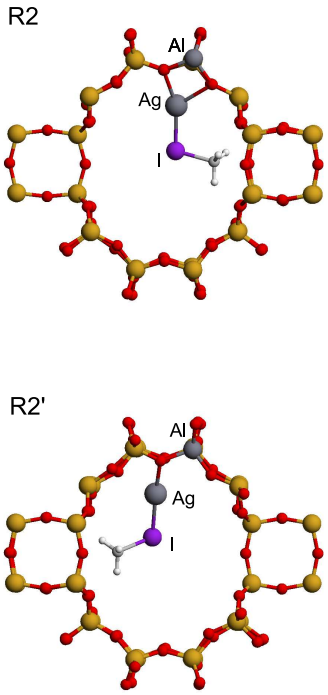

Figure 9: Comparison of relaxed adsorption complexes formed upon adsorption of iodomethane on Ag-MOR. The structure R2 corresponds to the zero-temperature ground-state, while the structure R2' was obtained by relaxation of a typical configuration generated by MD at 373 K.

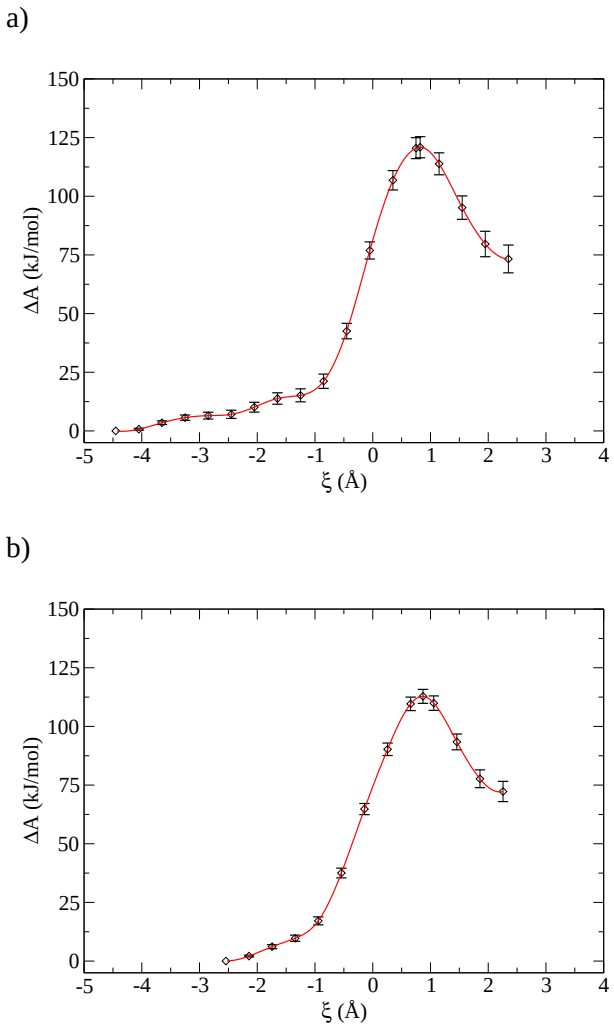

Figure 10: Free energy profiles for the CH_3I dissociation on Ag^+ in MOR: reaction involving a single reactant molecule (a) and two reactant molecules (b). The negative values of reaction coordinate (ξ) correspond to reactant while the positive values to product configurations.

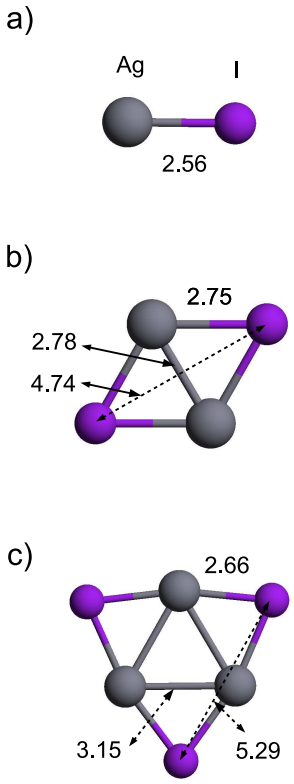

Figure 11: Geometries of relaxed clusters $(AgI)_n$ (n=1,2,3) created spontaneously in the main channel of MOR during a MD run at T=373 K: monomer (a), dimer (b), and trimer (c). All configurations are linear or planar, selected interatomic distances (Å) are displayed.

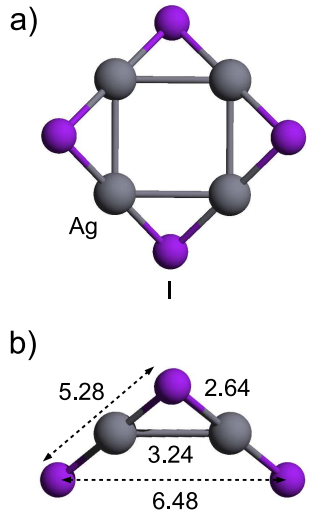

Figure 12: Top (a) and side (b) views on relaxed geometry of cluster $(AgI)_4$ formed spontaneously in the main channel of MOR. Selected interatomic distances are in Å.

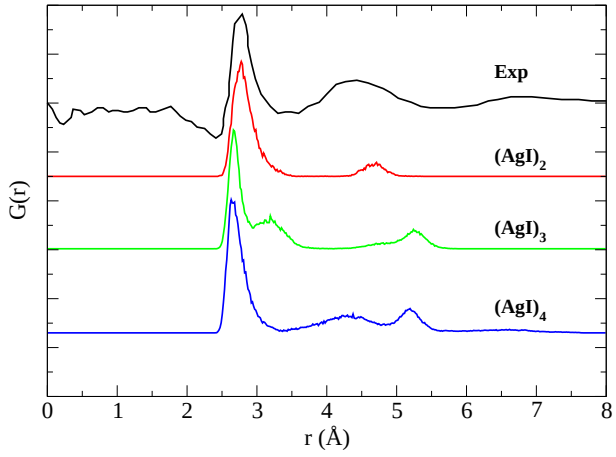

Figure 13: Comparison of experimental[14] and theoretical radial distribution functions (G(r)) determined for AgI formed in MOR. The theoretical G(r) has been computed for the clusters $(AgI)_2$, $(AgI)_3$, and $(AgI)_4$ using MD at T=373 K.